MRS Advances (2024) 9:391–396
https://doi.org/10.1557/s43580-024-00835-y

ORIGINAL PAPER

Investigation of kinetics and mechanisms of metallic beryllium corrosion for the management of radioactive wastes

Andrey Bukaemskiy[1] · Sebastien Caes[2] · Giuseppe Modolo[1] · Guido Deissmann[1] · Dirk Bosbach[1]

Received: 4 January 2024 / Accepted: 21 March 2024 / Published online: 12 April 2024

Abstract

Activated beryllium wastes are produced by the nuclear industry and have to be managed as radioactive waste during decommissioning and dismantling of nuclear facilities. One potential approach to the management of these wastes is their encapsulation and stabilization in cementitious matrices. The main issue with this conditioning is aqueous corrosion, leading to the hydrogen production and potential crack formation leading to a loss of confinement. To evaluate the suitability of different cement formulations, such as Ordinary Portland Cement (OPC) or magnesium phosphate cement for encapsulation of metallic beryllium, the corrosion behaviour of beryllium metal was investigated in solutions with different pHs. In alkaline solutions representative of OPC pore fluids (i.e. NaOH solutions with pH between 12.5 and 14), corrosion rates increase drastically with increasing pH. Investigations of the surface of the corroded beryllium samples by scanning electron microscopy indicate that pitting corrosion is the main corrosion mechanism under these conditions.

Introduction

Metallic beryllium is employed in a wide range of nuclear applications, for example, as moderator, reflector, or fuel cladding in thermal reactors, due to its low neutron-capture cross-section and high potential for elastic neutron scattering [1–3]. Moreover, it is also under consideration as interesting material for future fusion power reactors (e.g. as first wall) [4–6]. Neutron irradiation of beryllium during utilization in fission and fusion reactors entails the accumulation of significant amounts of short- and long-lived activation products (e.g. ^{3}H formed from ^{9}Be via $^{9}\mathrm{Be}(n,\alpha)^{6}\mathrm{He}\rightarrow{}^{6}\mathrm{Li}(n,\alpha)^{3}\mathrm{H}$, and ^{10}Be, as well as activation products of impurity elements, such as ^{14}C, ^{41}Ca, ^{60}Co, and ^{239}Pu), requiring its disposal as radioactive waste after decommissioning. One strategy for the management of low- and intermediate-level radioactive metallic wastes is their encapsulation in cementitious matrices [7–9]. Reactive metallic wastes produced by nuclear activities (such as aluminium, magnesium, or beryllium) may react with cement hydration phases or the pore water, thus having detrimental effects on the conditioning material [10]. A major issue is the corrosion of the metal resulting in the release of hydrogen, which can lead to cracking and gas driven transport of radionuclides out of the waste package, impairing the confinement of the radionuclides. However, data on the corrosion and reactivity of metallic beryllium in the disposal environment (e.g. with respect to H_2 evolution) are scarce [11].

The physico-chemical aspects of the passivation and degradation of beryllium in aggressive media have been investigated by various authors using open-circuit potential measurements and electrochemical impedance spectroscopy [11–13]. However, literature data on direct measurements of beryllium corrosion rates in aqueous solutions are scarce and apparently estimates rather than accurately measured values. Moreover, they are available only for neutral and slightly acidic conditions and not for the highly alkaline conditions prevailing in many cementitious materials based on Ordinary Portland Cement (OPC) [14, 15]. Thus, within the frame of the collaborative EC-funded Horizon 2020 project PREDIS (Predisposal management of radioactive waste) we investigated the corrosion behaviour of metallic beryllium in solutions with different pH and composition, simulating potential encapsulation matrices, such as OPC or magnesium phosphate cement (MPC), the latter characterized by

✉ Andrey Bukaemskiy
a.bukaemskiy@fz-juelich.de

[1] Forschungszentrum Jülich GmbH, Institute of Energy and Climate Research – Nuclear Waste Management (IEK-6), Wilhelm-Johnen Straße, 52428 Jülich, Germany

[2] Belgian Nuclear Research Centre (SCK CEN), Institute for Sustainable Waste & Decommissioning, Boeretang 200, 2400 Mol, Belgium

distinctly lower pore solution pH than OPC-based materials. Corrosion rates of metallic beryllium samples were determined experimentally using gravimetric methods (weight loss) combined with the determination of beryllium concentrations in solution via ICP-MS. The obtained results are compared with results derived by the H_2 release under similar conditions. Moreover, detailed studies of pristine and corroded metal surfaces were carried out using scanning electron microscopy (SEM) combined with energy-dispersive X-ray spectroscopy (EDS) providing insights into corrosion mechanisms and the possible initiation places for pit corrosion in dependence of solution composition.

Materials and methods

Beryllium foil (Alfa Aesar, 99.8% purity) with a thickness of 0.25 mm was used as initial material to allow for microscopical investigation of corrosion features and to avoid the risks associated with the use of beryllium powder due to its high toxicity. The density of the Be foil was measured by hydrostatic weighing in water and equals 1.842 ± 0.001 g/cm^3, correlating well with reference data [16]. Aluminium foils (Alfa Aesar, 99.997% purity) with a thickness of 0.25 mm were also used in this work for comparative analysis of corrosion properties since an analogous corrosion behaviour has been assumed in the past. For experiments on metal corrosion, Be and Al samples with a size of approximately 1.7×3.2 cm were mechanically cut out. The initial samples were cleaned by rinsing them with acetone and ethanol and were treated with HCl (0.5 M) solution (around 1 min) as recommended in [11]. Then, they were rinsed thoroughly with demineralized water and dried with a tissue paper.

The corrosion experiments were carried out in tightly sealed plastic containers with a volume of 0.5 L under air atmosphere. Three NaOH solutions with pH values equal to 12.6, 13.2, and 14.0, respectively, were used; the initial volume of the solution was 250 mL. The total duration of the corrosion experiments for beryllium was 30 days, and the sampling periodicity was once every 1–2 days. After sampling, the solution was not supplemented; the change in solution volume was taken into account in the calculation of the corrosion rates. The Be samples were removed from the solution, thoroughly washed with demineralized water, carefully dried with a soft tissue paper following the procedure recommended by Bouhier et al. [11], and then weighted. In addition, 2 mL of the leaching solution was abstracted for subsequent determination of beryllium concentrations using ICP-MS (Elan 6100 DRC).

The corrosion of beryllium in water-based solutions is the sum of two electrochemical reactions, oxidation and reduction and proceeds in circumneutral conditions according to the following equation:

$$\mathrm{Be} + 2\mathrm{H_2O} \rightarrow \mathrm{Be(OH)_2} + \mathrm{H_2}. \quad (1)$$

Beryllium corrosion results in the release of hydrogen and the formation of $Be(OH)_2$, which can form a passivating layer on the metal (i.e. similar to Al hydroxides on aluminium) and has its lowest solubility under neutral to slightly alkaline conditions, but is more soluble under highly alkaline conditions [17]. According to the solubility diagram presented in [17], $Be(OH)_2$ is in equilibrium with $Be(OH)_3^-$ and $Be(OH)_4^{2-}$ at higher pH values (above 11).

Therefore, Be corrosion rates can be determined by three direct experimental methods, namely, measurements of (a) mass loss of the initial sample (ML), (b) the concentration of beryllium in solution (ICP-MS), and (c) the amount of hydrogen released (H_2 release). Ideally, the values of the corrosion rates determined by these three methods should be equal.

The presence of a hydroxide layer on the metal surface leads to an underestimation of the amount of corroded metal by measuring ML:

$$\mathrm{ML} = -m_{\mathrm{Be}}^{\mathrm{cor}} + R m_{\mathrm{Be}}^{\mathrm{s}}, \quad (2)$$

where $m_{\mathrm{Be}}^{\mathrm{cor}}$ is the mass of corroded beryllium and $m_{\mathrm{Be}}^{\mathrm{s}}$ the mass of beryllium being in the form of hydroxide on the sample surface, and the coefficient $R = 4.774$ equals the ratio of the molecular weights of the hydroxide and the metal, respectively.

The mass of corroded beryllium consists of two components—the mass of Be as hydroxide on the metal surface and that dissolved in solution, $m_{\mathrm{Be}}^{\mathrm{sol}}$.

$$m_{\mathrm{Be}}^{\mathrm{cor}} = m_{\mathrm{Be}}^{\mathrm{s}} + m_{\mathrm{Be}}^{\mathrm{sol}}. \quad (3)$$

Using Eqs. (2) and (3), an equation can be obtained for the mass of corroded beryllium which consists of two experimentally measured values—the concentration of beryllium in solution (determined by ICP-MS) and mass loss (ML).

$$m_{\mathrm{Be}}^{\mathrm{cor}} = \frac{R m_{\mathrm{Be}}^{\mathrm{sol}} + \mathrm{ML}}{R - 1}. \quad (4)$$

To measure the H_2 release with time, Be samples were immersed in alkaline solutions in a leak-tight container. The headspace of the container was injected on a regular basis in a Shimadzu GC-2010 Plus type gas chromatograph, using a ShinCarbon ST column and a Barrier Discharge Ionization Detector. Moreover, detailed studies of the morphological features of the structure of pristine and corroded metal surfaces were carried out using a FEI model Quanta 200F SEM equipped with a Genesis 4000 EDS analyser.

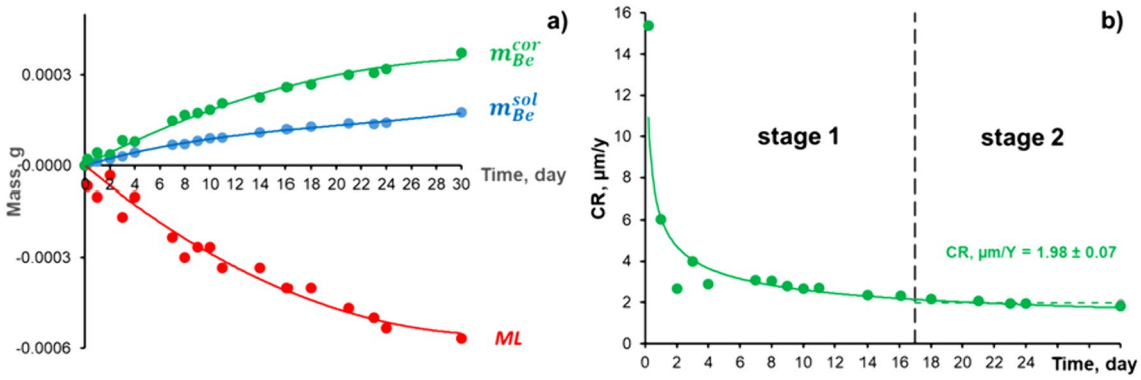

Fig. 1 **a** Sample mass loss (ML, red line), mass of beryllium in solution (m_{Be}^{sol}, blue line), and calculated mass of corroded beryllium metal (m_{Be}^{sol}, green line) in a representative experiment at pH 13.2; **b** evolution of corrosion rate (CR) at pH 13.2 as function of exposure time

Results and discussion

Corrosion rates

In Fig. 1a, the measured mass loss (ML) and amounts of beryllium in solution (m_{Be}^{sol}) are shown for a representative experiment performed at pH 13.2 as function of experimental duration. The mass of the sample decreases and the content of Be in solution (blue line) increases monotonically with increasing duration of the experiment. Based on these data, the corrosion rates (CR) were calculated; the results are presented in Fig. 1b. The corrosion rate decreased steeply with time (stage 1) and reached an almost constant value after 17 days (stage 2). The average corrosion rates were calculated specifically for the second stage and is equal to 1.98 ± 0.07 µm/year at pH 13.2.

The results of corrosion rate measurements at various pH values are presented in Fig. 2 and summarized in Table 1. Under alkaline conditions, the corrosion rates of Be in logarithmic coordinates increase linearly with increasing pH and correlate well with the results obtained by measuring the H_2 release. The literature data on beryllium corrosion in aqueous solutions [14, 15] are included in Fig. 2 for comparison. It should be noted that these data are for neutral and slightly acidic solutions and estimates of the corrosion rates rather than accurately measured values.

For comparison, the measured corrosion rates of metallic Al determined under similar conditions are also included in Fig. 2 and Table 1. Aluminium corrosion at neutral or slightly acidic/alkaline conditions results in the formation of aluminium hydroxides (e.g. $Al(OH)_3$, AlOOH), which are sparingly soluble in water and form a protective layer under these conditions, but are soluble at low and high pH, respectively [18]. Therefore, the values of the Al corrosion rates under highly alkaline conditions were determined by the mass loss. The measured rates show also a strong increase with increasing pH, in good agreement with literature data

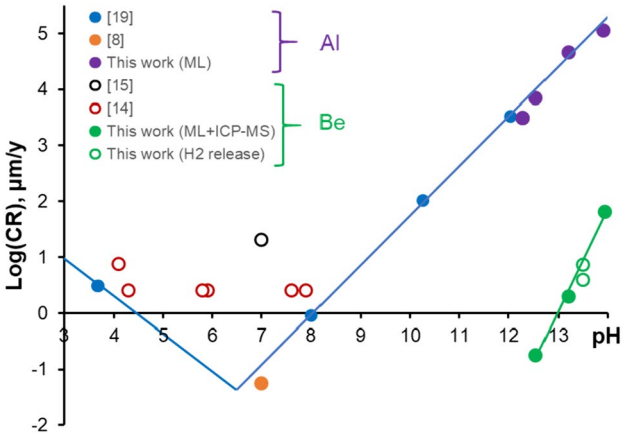

Fig. 2 Corrosion rates of metallic Be and Al determined in this study compared to available literature data [8, 14, 15, 19]

Table 1 Corrosion rates (CR) of metallic beryllium and aluminium in NaOH solutions of different pHs

pH	Corrosion rate (*CR*), µm/year		CR_{Al}/CR_{Be}
	Be	Al	
12.6	0.18 ± 0.02	6940 ± 20	38556
13.2	1.98 ± 0.07	45730 ± 50	23096
14.0	64.4 ± 1.4	112800 ± 100	1752

[19], and are significantly higher than the corrosion rates of metallic beryllium. The ratios of corrosion rates for metallic aluminium and beryllium (CR_{Al}/CR_{Be}) reveal that the corrosion rates of metallic aluminium are 3 to 4 orders of magnitude higher than those of beryllium (cf. Table 1). This indicates that metallic Al is not a suitable analogue to assess the behaviour of Be under highly alkaline cementitious conditions.

The decrease in Be corrosion rates with time is presumably due to a hydroxide layer forming on the surface of the Be metal, which is confirmed by our microscopic studies (cf. "Scanning electron microscopy observations" section). The good adhesion of Be hydroxide to the metal surface is probably due to similarities of their crystal lattice parameters ($a_{Be} = 2.287$ Å [20] $\approx 0.25(a+b)_{Be(OH)2} = 2.288$ Å [21]). Moreover, the hydroxide occupies a volume 4.54 times larger than that of the metal consumed in forming the hydroxide (Pilling–Bedworth ratio). Thus, being in expansion, the oxide does not have any tendency to spall. It can be assumed that at stage 1 there is a predominant dissolution of Be from "defective" sites of the samples and a protective layer of hydroxide just begins to form. At stage 2, a certain steady state is reached between the formation of a protective layer of hydroxide and the dissolution of metallic beryllium. The presence of a protective layer of hydroxide on the surface of the material probably determines the higher corrosion resistance of metallic beryllium in comparison to aluminium under hyperalkaline conditions.

Scanning electron microscopy observations

According to [22], corrosion of beryllium metal starts at sensitive points which comprise crystallographic defects, cavities, or scratches in the metal surface and/or impurity inclusions mainly localized along grain boundaries [23]. Figure 3a shows the surface of the original Be foil with two types of mechanical defects visible on the surface of the beryllium metal, namely numerous elongated linear defects (scratches) due to mechanical processing (rolling) and, locally present, rather deep defects (cavities). Impurity

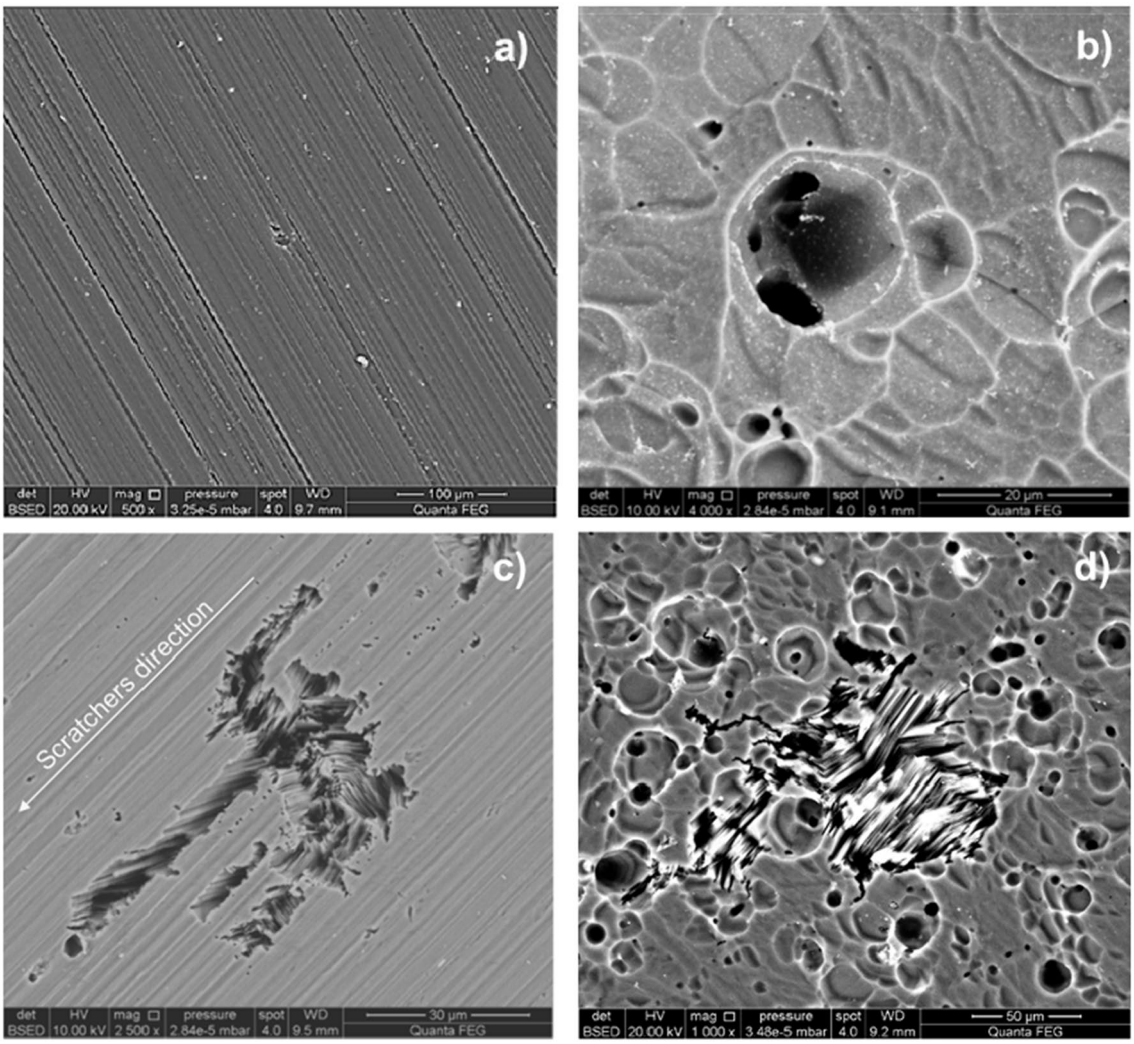

Fig. 3 **a** SEM surface images (back-scattered electron images) of a pristine Be sample with scratches from mechanical processing and impurity inclusions (white spots); **b** Be hydroxide layer formed on a Be sample corroded at pH 14.0; **c** corrosion pits in Be metal corroded at pH 13.2 and **d** pH 14.0

inclusions are also present in the material with sizes varying between 0.4 and 3.5 µm (cf. Fig. 3a). These inclusions were identified by SEM–EDS as BeO, Be_2C, silicon (Si), and various intermetallic phases, such as Be/Cr/Al/Mn, Si_2Cr, and Al/Mn/Si/Cr.

Figure 3b shows that the surface of the corroded Be metal samples is uniformly covered by a thin layer of $Be(OH)_2$. Moreover, two types of corrosion pits could be observed in the corroded samples: (1) large (40–200 µm) pits with an elongated shape, where the direction of pit elongation coincides with the direction of the original scratches (Fig. 3c) and (2) smaller (3–30 µm) corrosion pits characterized by a spherical (cylindrical) shape (cf. Fig. 3d).

Apparently, the large corrosion pits formed at the sites of originally present scratches and cavities. They have a complex morphology consisting of pit walls and parallel plates, which can be explained by the differing dissolution rates of different crystallographic orientations of the Be grains [24]. The small corrosion pits are also located on the tops of scratches and irregularities of the original Be metal. This indicates that mechanical defects (cavities, edges of scratches) in the initial beryllium foil are the initiation places for pitting corrosion.

Conclusion

In the present work, the corrosion of metallic beryllium in highly alkaline aqueous solutions mimicking the pH of pore waters encountered in OPC-based cementitious materials has been studied by various methods. Corrosion rates determined by combining mass loss and aqueous Be concentrations showed a strong increase of Be corrosion rates with increasing pH in hyperalkaline solutions (pH > 12), with good correspondence to corrosion rates determined from the release of hydrogen gas. Detailed microscopic studies of the material before and after corrosion suggest pitting corrosion as one important mechanism of beryllium metal corrosion at highly alkaline solutions. Mechanical defects (cavities, edges of scratches) on the initial beryllium foil surface acted as the initiation places for pit corrosion. Complementary experiments performed with Al foils under similar conditions showed that the corrosion rates of Al under highly alkaline conditions are several orders of magnitude higher than those of Be metal, suggesting that Al is not a suitable surrogate for the evaluation of the behaviour of metallic Be in cementitious environments. The results of this study show that Be metal is distinctly less reactive than Al under highly alkaline conditions, indicating that conditioning of metallic Be in cementitious matrices is a viable option. However, to limit generation of hydrogen gas and associated deleterious effects, cement formulations leading to (initially) very high pH pore solutions (pH > 13) should be avoided (cf. [11]). Further work will be dedicated to the investigation of the behaviour of metallic Be encapsulated in MPC-based matrices, where lower long-term corrosion rates are expected due to the slightly alkaline pH.

Acknowledgments This project has received funding from the Euratom research and training programme 2014–2018 under Grant Agreement No. 945098 (PREDIS).

Author's contributions AB carried out the experiments, analysis, and validation of the data obtained, development of the corrosion model, and took the lead in writing the manuscript; SC performed the additional experiments; GM and GD were involved in planning and supervised the work; and DB supervised the project. All authors discussed the results and commented on the manuscript.

Funding Open Access funding enabled and organized by Projekt DEAL. Open Access funding enabled by the Deutsche Forschungsgemeinschaft (DFG, German Research Foundation) – 491111487 and organized by the Projekt DEAL.

Data availability The data generated during the current study are available from the corresponding author on reasonable request.

Declarations

Conflict of interest The authors declare that they have no known competing financial interests or personal relationships that could have appeared to influence the work reported in this paper.

References

1. B.G. Naik, N. Sivasubramanian, Miner. Process. Extr. Metall. Rev. **13**, 243–251 (1994). https://doi.org/10.1080/08827509408914113
2. G.R. Longhurst, K. Tsuchiya, C.H. Dorn, S.L. Folkman, T.H. Fronk, M. Ishihara, H. Kawamura, T.N. Tranter, R. Rohe, M. Uchida, E. Vidal, Nucl. Technol. **176**, 430–441 (2011). https://doi.org/10.13182/NT11-A13318
3. K. Kurosaki, S. Yamanaka, in *Comprehensive Nuclear Materials*, 2nd edn, ed. by R.J.M. Konings, R.E. Stoller (Elsevier, Amsterdam, 2020). https://doi.org/10.1016/B978-0-12-803581-8.11747-3
4. G. Federici, R. Doerner, P. Lorenzetto, V. Barabash, in *Comprehensive Nuclear Materials*, ed. by R.J.M. Konings (Elsevier, Amsterdam, 2012). https://doi.org/10.1016/B978-0-08-056033-5.00121-X

5. M. Nakamichi, J.-H. Kim, M.M. Nakamura, T. Shibayama, C.K. Dorn, C. Vladimir, D.V. Bachurin, C. Stihl, P. V. Vladimirov, in *Comprehensive Nuclear Materials*, 2nd edn, ed. by R.J.M. Konings, R.E. Stoller (Elsevier, Amsterdam, 2020). https://doi.org/10.1016/B978-0-12-803581-8.11673-X
6. J.S. Park, X. Bonnin, R. Pitts, Nucl. Fusion **61**, 016021 (2021). https://doi.org/10.1088/1741-4326/abc1ce
7. F. Glasser, Application of inorganic cements to the conditioning and immobilisation of radioactive wastes, in *Handbook of advanced radioactive wastes conditioning technologies* . ed. by M.I. Ojovan (Woodhead Publishing, Sawston, 2011), pp.67–135. https://doi.org/10.1533/9780857090959.1.67
8. C. Cau-dit-Coumes, D. Lambertin, H. Lahalle, P. Antonucci, C. Cannes, S. Delpech, J. Nucl. Mater. **453**, 31–40 (2014). https://doi.org/10.1016/j.nucmat.2014.06.032
9. S. Delpech, C. Cannes, N. Barré, Q.T. Tran, C. Sanchez, H. Lahalle, D. Lambertin, S. Gauffinet, C. Cau-dit-Coumes, J. Electrochem. Soc. **164**, C717–C727 (2017). https://doi.org/10.1149/2.0211713jes
10. R. Perona, C. Fernández-García, I. García-Lodeiro, M. Criado, J.M. Bastidas, M.C. Alonso, J. Nucl. Mater. **582**, 154501 (2023). https://doi.org/10.1016/j.jnucmat.2023.154501
11. P. Bouhier, C. Cannes, D. Lambertin, C. Grisolia, D. Rodrigues, S. Delpech, J. Nucl. Mater. **559**, 153464 (2022). https://doi.org/10.1016/j.jnucmat.2021.153464
12. E. Gulbrandsen, A.M.J. Johansen, Cor. Sci. **36**(9), 1523–1536 (1994). https://doi.org/10.1016/0010-938X(94)90050-7
13. M.A. Hill, D.P. Buft, R.S. Litlard, J. Electrochem. Soc. **145**, 2799–2806 (1998). https://doi.org/10.1149/1.1838717
14. J.L. English, *The metal beryllium* (American Society for Metals, Cleveland, 1955)
15. R.J. Prochko, J.R. Myers, R.K. Saxer, Mater. Prot. **5**, 39–42 (1966)
16. K.A. Walsh, *Beryllium chemistry and processing* (ASM International, Geauga, 2009)
17. C. Cannes, P. Bouhier, D. Lambertin, C. Grisolia, D. Rodrigues, S. Delpech, J. Electroanal. Chem. **950**, 117879 (2023). https://doi.org/10.1016/j.jelechem.2023.117879
18. K. Vargel, *Corrosion of aluminium* (Elsevier, Amsterdam, 2004)
19. A.Y. Chatalov, D. Akad Nauk, SSSR **86**, 775–777 (1952)
20. R.W.G. Wyckoff, *Crystal structures*, vol. 1 (Interscience Publishers, New York, 1963)
21. R. Stahl, C. Jung, H.D. Lutz, W. Kockelmann, H. Jacobs, Z. Anorg. Allg. Chem. **624**, 1130–1136 (1998)
22. J.M. West, *Electrodeposition and corrosion processes* (Plenum Press, New York, 1970)
23. J.S. Punni, M.J. Cox, Cor. Sci. **52**, 2535–2546 (2010). https://doi.org/10.1016/j.corsci.2010.03.024
24. R.S. Lillard, J. Electrochem. Soc. **148**, B1–B11 (2001). https://doi.org/10.1149/1.1344526